Pergamon

Int. J. Heat Mass Transfer. Vol. 39, No. 6, pp. 1121–1133, 1996

0017-9310/96 $15.00+0.00

0017-9310(95)00207-3

Amplitude effect on convection induced by time-periodic horizontal heating

B. V. ANTOHE and J. L. LAGE†

Mechanical Engineering Department, Southern Methodist University, Dallas, TX 75275-0337, U.S.A.

(*Received* 13 *February* 1995 *and in final form* 20 *June* 1995)

Abstract—Heat and momentum transport is investigated theoretically and numerically considering a rectangular enclosure filled with clear fluid or with fully saturated porous medium, under time-periodic horizontal heating. Numerical simulations, of various configurations, indicate that the natural convection activity within the enclosure peaks at several discrete frequencies, with the climax attained at a heating frequency referred to as *resonance frequency*. A general theory for predicting this resonance frequency is developed from the natural frequency of the flow circulating inside the enclosure. The resonance frequency can be calculated by solving a system of non linear equations, function of the averaged Rayleigh number, the Prandtl number, the enclosure aspect ratio, the heating amplitude, and the Darcy number for the porous medium case. Theoretical predictions agree well with numerical results. It is shown that the convection intensity within the enclosure increases linearly with heating amplitude for a wide range of parameters. Moreover, the flow response to pulsating heat is continuously enhanced as the system becomes more permeable. Time evolution graphs, phase-plane portraits, and streamlines highlight several distinct phases of the periodic heating process.

INTRODUCTION

Natural convection flow induced by time periodic thermal boundary conditions is a subject of increasing interest. This area of research is attractive to those who: (1) desire to unravel the physical nuances of the highly non linear transport phenomena produced by periodic heating–cooling; (2) are challenged by the need of predictive theoretical models of system's response; (3) anticipate the potential for practical engineering applications, as for instance in phase-change processes [1–3], energy systems [4, 5], building insulation and fire protection techniques [6, 7], grain storage design [8] and hazardous thermo-chemical spreading [9].

The development of theoretical models allied with numerical simulations and experimental evidence is forming a solid basis for the advancement of knowledge in this field. An excellent state-of-the-art review was presented recently by Fusegi and Hyun [10]. Noteworthy are the studies dealing with clear fluid systems by Yang *et al.* [11], Kazmierczak and Chinoda [12], Lage and Bejan [13], Mantle *et al.* [14] and Lage [15]. The systems considered in these studies are rectangular cavities subjected to horizontal or vertical temperature gradients. A discovery of practical interest is the time-averaged heat transfer increase by intermittent thermal boundary conditions as compared with the heat transfer obtained with steady-state boundary condition. Another is the fundamental phenomenon of flow resonance characterized by a surge in the convective activity within an enclosure.

Studies dealing with convection in a fluid saturated porous medium system subjected to time periodic boundary condition are scarce. Caltagirone [16], Chhuon and Caltagirone [17], Rudraiah and Malashetty [18] investigated the stability or onset of convection in a fluid saturated porous medium layer under periodic vertical temperature gradient. A study of the corresponding supercritical (convection) regime was presented recently by Kazmierczak and Muley [19]. A unique theoretical addition was the work by Nield [20] on time-periodic volumetric heating of a fluid saturated porous medium. Convection induced by a fixed-amplitude, time-periodic, horizontal heat flux imposed on a saturated porous medium enclosure was studied by Antohe and Lage [21]. They demonstrated that the concept of flow resonance extends also for moderate and high permeability porous systems, being negligible on systems with low permeability.

Kazmierczak and Mulley [19] showed that the thermal oscillation amplitude is a factor on the heat transfer enhancement of vertically heated enclosures. The present work investigates the amplitude effect on the convection within a clear fluid, or a fluid saturated porous medium, rectangular enclosure heated horizontally in a time-periodic fashion. Numerical simulations are carried out covering the entire heat frequency spectrum. For the clear fluid configuration (no porous matrix), the heat-flux-based Rayleigh number is varied from 10^7 to 10^9. The fluid saturated porous

†Author to whom correspondence should be addressed.

NOMENCLATURE

A	heat pulsation amplitude, Fig. 1
Da	Darcy number, equation (7)
f, F	dimensional and non-dimensional frequencies, $F = 1/(2\Omega)$
g	acceleration of gravity [m s^{-2}]
H	enclosure height [m]
i	iteration index
I	Forchheimer inertia coefficient, equation (8)
L	enclosure length [m]
J	viscosity ratio, equation (6)
k	thermal conductivity [W m K^{-1}]
K	permeability [m^2]
Nu	Nusselt number, equations (10) and (11)
p, P	dimensional and non-dimensional pressures, equation (5)
Pr	Prandtl number, equation (7)
q'', Q''	dimensional and non-dimensional heat fluxes, equation (8)
Ra	Rayleigh number, equation (8)
t	time [s]
T	temperature [K]
u, v	horizontal and vertical seepage (Darcy) velocity components [m s^{-1}]
U, V	non-dimensional horizontal and vertical velocity components, equation (5)
x, y	horizontal and vertical coordinates [m]
X, Y	non-dimensional horizontal and vertical coordinates, equation (5)
W	non-dimensional volume-averaged velocity, equation (23).

Greek symbols

α	thermal diffusivity, equation (7) [m^2 s^{-1}]
β	isobaric coefficient of thermal compressibility [K^{-1}]
δ	velocity layer thickness scale
Δ	difference
ε	dummy variable, equation (21)
ϕ	porosity
λ	volumetric specific heat ratio, equation (7)
μ	dynamic viscosity [kg m^{-1} s^{-1}]
ν	kinematic viscosity [m^2 s^{-1}]
θ	non-dimensional temperature, equation (6)
ρ	density [kg m^{-3}]
τ	non-dimensional time, equation (6)
ϑ_{ij}	local (i,j) volume, equation (23)
ξ	auxiliary function
Ω	heating non-dimensional half-period, Fig. 1
Ψ	streamfunction.

Subscripts

C	isothermal cold wall
cr	critical
D	porous modified
ΔT	temperature difference
f	fluid
h	high-heating regime
H	heated wall
l	low-heating regime
m	reference value
M	mid vertical plane
max	maximum value
s	porous medium (fluid and solid matrix)
ss	steady state
v	flow
o	initial
θ	temperature.

Superscripts

$(^-)$	surface averaged.

medium configuration is studied considering Darcy number values from 10^{-6} to 10^{-2}, with Darcy-modified Rayleigh number from 10^4 to 10^8. The Prandtl number is fixed and equal to 7. The non-dimensional heat amplitude varies from 0.2 to a maximum value equal to 2, beyond which the heating cycle degenerates with periods of effective cooling.

PHYSICAL MODEL

Consider an enclosure, as depicted in Fig. 1 (top), filled with a fully saturated solid homogeneous and isotropic porous matrix or with a clear (of any solid matrix) fluid. In either case, the fluid is Newtonian with constant properties, and the Oberbeck–Boussinesq approximation is considered valid. For the fluid saturated porous matrix configuration, the fluid and porous matrix are assumed to be in thermal equilibrium throughout the heating process. The left wall of the enclosure is maintained at a constant uniform-temperature. A periodic heat flux, following the time evolution shown in Fig. 1 (bottom), is applied at the right wall. All other surfaces of the enclosure are assumed adiabatic.

It is convenient to introduce the non-dimensional, time-dependent, general conservation of mass, momentum, and energy equations for a fluid saturated porous medium system [22, 23], written in Cartesian coordinates:

$$\frac{\partial U}{\partial X} + \frac{\partial V}{\partial Y} = 0 \tag{1}$$

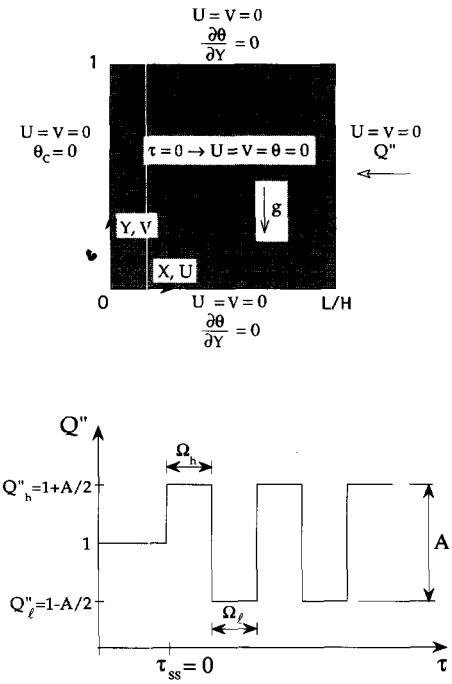

Fig. 1. Model of physical system and boundary conditions (top); square wave heating (bottom).

$$\frac{DU}{D\tau} = -\frac{\partial P}{\partial X} + \phi\, Pr\, J\nabla^2 U - \phi^2 \frac{I}{Da}(U^2+V^2)^{1/2}U - \phi^2 \frac{Pr}{Da}U \quad (2)$$

$$\frac{DV}{D\tau} = -\frac{\partial P}{\partial Y} + \phi\, Pr\, J\nabla^2 V - \phi^2 \frac{I}{Da}(U^2+V^2)^{1/2}V - \phi^2 \frac{Pr}{Da}V + \phi^2\, Ra\, Pr\,\theta \quad (3)$$

$$\frac{\lambda}{\phi}\frac{\partial\theta}{\partial\tau} + U\frac{\partial\theta}{\partial X} + V\frac{\partial\theta}{\partial Y} = \nabla^2\theta. \quad (4)$$

The dimensionless variables (corresponding dimensional quantities are listed in the nomenclature) are:

$$(X, Y) = \frac{(x, y)}{H} \quad (U, V) = \frac{(u, v)}{\alpha_s/H}$$

$$P = (p+\rho g y)\frac{\phi^2 H^2}{\rho_f \alpha_s^2} \quad (5)$$

$$\theta = \frac{T-T_o}{q''_m H/k_s} \quad \tau = \frac{t-t_{ss}}{\phi H^2/\alpha_s} \quad J = \frac{\mu_s}{\mu} \quad (6)$$

$$\lambda = \frac{(\rho c)_s}{(\rho c)_f} \quad Pr = \frac{\nu}{\alpha_s} \quad \alpha_s = \frac{k_s}{(\rho c)_f} \quad Da = \frac{K}{H^2} \quad (7)$$

$$Ra = \frac{g\beta q''_m H^4}{\nu\alpha_s k_s} \quad I = 1.75\left(\frac{Da}{150\phi^3}\right)^{1/2} \quad Q'' = \frac{q''}{q''_m}. \quad (8)$$

The general transport equations are convenient because they reduce to the Navier–Stokes equations for modeling transport phenomena in a clear fluid system by setting $Da \to \infty$, $\phi = \lambda = J = 1$, and making all porous medium properties, $(\ )_s$, equal to the corresponding fluid property, $(\ )_f$.

The term $D(\ )/D\tau$ of equations (2) and (3) represents the total derivative, $\partial(\ )/\partial\tau + U\partial(\ )/\partial X + V\partial(\ )/\partial Y$. Parameter J, equation (6), accounts for the effective viscosity of the fluid saturated porous medium [24]. The expression for the inertia parameter, I, shown in equation (8), is obtained by invoking the Ergun [25] model. The Rayleigh number defined in equation (8) is based on the cycle-averaged heat flux, q''_m; the instantaneous time-dependent Rayleigh number is then equal to $Ra\,Q''$. The porous-modified, heat-flux-based Rayleigh number, Ra_D, is defined as equal to $Ra\,Da$.

For a porous medium configuration, the time dependent inertia term kept in both momentum equations (2) and (3) is negligible for most practical situations (the time of transient decay is proportional to $Da/(\phi^2 Pr)$ for Darcy flow, and to $Da^{3/4}/(\phi^{3/2} Ra_D\, Pr)^{1/2}$ for Forchheimer flow, [26]). However, for moderate to high Darcy number values, as considered in the present study, the transient flow inertia terms should not be neglected *a priori*.

In both clear fluid and porous medium configurations, the enclosure is saturated with initially motionless and isothermal fluid. The left wall of the enclosure is set at a constant temperature, θ_C, equal to the initial temperature of the system, $\theta_o = 0$. A constant heat flux, $Q'' = 1$, is then imposed on the right wall. The initial phase of the thermal process refers to the heating of the enclosed quiescent fluid until a steady convection regime is attained. At $\tau = 0$ (note that the non-dimensional time, equation (6), is zero when the system reaches steady state, $t = t_{ss}$), the system undergoes a second phase during which the dimensionless heat flux at right wall oscillates with amplitude A (Fig. 1).

According to the definition of dimensionless time, equation (6), and Fig. 1, the dimensional high-heating and low-heating time intervals are, respectively: $(\Delta t_h, \Delta t_l) = (\Omega_h, \Omega_l)\,\phi H^2/\alpha_s$, for the porous case, and $(\Delta t_h, \Delta t_l) = (\Omega_h, \Omega_l)H^2/\alpha_f$, for the clear fluid case. Equal high-heating and low-heating periods are assumed here, $\Omega_h = \Omega_l = \Omega$, therefore, the non-dimensional heating frequency is: $F = 1/(2\Omega)$. Notice that by definition of the non-dimensional pulsating heat flux, equation (8), the system is never cooled during the heat pulsating process unless A is larger than 2. At $A = 2$, high-heating periods are intercalated with adiabatic periods.

Three parameters are chosen to help understand the heat-amplitude effect on convection, respectively: right (heating) wall, instantaneous, surface-averaged temperature, $\bar{T}_H$; instantaneous, surface-averaged, left (isothermal) wall heat flux, $\bar{q}''_C$; and instantaneous, surface-averaged, heat transfer rate through an imaginary vertical plane positioned at the middle of

the enclosure, $\bar{q}'_M$. The corresponding non-dimensional quantities are:

$$\bar{\theta}_H = \int_0^1 \theta|_{X=L/H}\,dY \tag{9}$$

$$Nu_C = \frac{\bar{q}''_C}{q''_m} = \int_0^1 \left.\frac{\partial\theta}{\partial X}\right|_{X=0} dY \tag{10}$$

$$Nu_M = \frac{\bar{q}''_M}{q''_m} = \int_0^1 \left(U\theta - \frac{\partial\theta}{\partial X}\right)_{X=L/(2H)} dY. \tag{11}$$

From the heat-flux-based Rayleigh number, equations (8) and (9), a temperature-based Rayleigh number can be defined and written as

$$Ra_{\Delta T} = \frac{g\beta(\bar{T}_H - T_C)H^3}{\nu\alpha_s} = \bar{\theta}_H Ra. \tag{12}$$

THEORETICAL ANALYSIS

A theory to obtain an estimate of the heating frequency that leads to natural convection resonance is now presented. As indicated by Antohe and Lage [21], flow resonance is expected to be induced when the heat pulsating frequency, f, coincides with the frequency of the flow wheel circulating within the enclosure, f_v. The result of this simple but powerful theoretical analysis is fundamental as it provides a base value around which a precise resonance frequency value can be searched by numerical simulations.

A theoretical representation of the flow wheel frequency, f_v, was introduced by Antohe and Lage [21] for clear fluid and porous medium configurations, assuming a single fluid circulating speed (valid during a complete pulse) based on the cycle-averaged Rayleigh number. Their approach led to a simple, closed-form solution for estimating the resonance frequency.

A more consistent and general theory can be developed by recognizing that different fluid circulating speeds are induced during each heating period of the pulse. The corresponding cycle-averaged velocity is different than the velocity induced by the cycle-averaged Rayleigh number (the velocity scale is a non linear function of the Rayleigh number). Although more laborious, this novel approach leads to a more accurate estimate of the resonance frequency by including the heating amplitude effect (the result presented by Antohe and Lage [21] is independent of the heating amplitude). The extra effort is translated, eventually, into fewer numerical simulations for establishing the precise resonance frequency of the system.

Each individual flow velocity, for each heating period (high-heating, low-heating), is scaled based on the respective instantaneous Rayleigh number, RaQ''. The cycle-averaged velocity scale is defined as the algebraic average of the individual high-heating and low-heating velocity scales. The dimensional circulating frequency scale is obtained by dividing the average velocity scale by the scaled distance traveled by a fluid pack per cycle within the enclosure (enclosure perimeter):

$$f_v \sim \frac{\left(\frac{v_h + v_l}{2}\right)}{2(H+L)}. \tag{13}$$

The same flow frequency scale in non-dimensional form is

$$F_v = \frac{1}{(\Omega_h + \Omega_l)} \sim \frac{V_h + V_l}{4\left(1 + \frac{L}{H}\right)}. \tag{14}$$

The velocity scales, V_h and V_l, are obtained by cross-differentiating the general momentum equations (2) and (3) to eliminate the pressure gradient term. The result, in a scaled form, is

$$\frac{V_{h,l}}{\Omega_{h,l}} + V_{h,l}^2 \sim -\phi J Pr \frac{V_{h,l}}{\delta_{h,l}^2} - \frac{0.143\phi^{1/2}}{Da^{1/2}} V_{h,l}^2 - \frac{\phi^2 Pr}{Da} V_{h,l} + \phi^2 Ra\, Pr\, \theta_{h,l} \left(\frac{\delta}{\delta_\theta}\right)_{h,l} \tag{15}$$

where $\theta_{h,l}$ is the high-heating or low-heating temperature scale. The high-heating or low-heating thermal boundary layer scale, $\delta_{\theta_{h,l}}$, is obtained from scaling the energy equation (4):

$$\delta_{\theta_{h,l}} \sim \frac{1}{\left[\left(\frac{\lambda}{\phi}\right)\frac{1}{\Omega_{h,l}} + V_{h,l}\right]^{1/2}} \tag{16}$$

provided $\delta_{\theta_{h,l}}$ of equation (16) be smaller than its upper bound $L/(2H)$.

The relationship between the thermal boundary layer and the velocity layer is, for a clear fluid system [27]: $(\delta_\theta/\delta)_{h,l} = \xi(Pr)^{1/2}$, with $\xi(Pr)$ equal to 1 for $Pr \geqslant 1$, or to Pr^{-1} for $Pr \leqslant 1$. Lage [28] showed that the same relationship is also valid for a porous medium system configuration provided the Prandtl number be replaced by the porous modified Prandtl number, as defined in equation (7). With the thermal boundary layer to velocity layer ratio, $(\delta_\theta/\delta)_{h,l}$, and equation (16), the momentum equation (15) is rearranged as:

$$V_{h,l}^2\left[1 + \phi J Pr\, \xi(Pr) + \frac{0.143\phi^{1/2}}{Da^{1/2}}\right] + V_{h,l}\left[\frac{1}{\Omega_{h,l}} + \frac{\lambda}{\Omega_{h,l}} J Pr\, \xi(Pr) + \frac{\phi^2 Pr}{Da}\right] - \phi^2 Ra\, Pr\, \xi(Pr)^{-1/2}\theta_{h,l} \sim 0. \tag{17}$$

Equation (17) is valid during both high and low heating periods. For equal heating periods $\Omega_h = \Omega_l = \Omega$, the distinction between high and low velocity scales is made by the temperature scale within each heating period. An adequate scale for $\theta_{h,l}$ during each heating period is the scale of the heating wall averaged tem-

perature $\bar{\theta}_H$ ($\bar{\theta}_{H_h}$ and $\bar{\theta}_{H_l}$). For a porous medium system, the averaged temperature scale of a vertical wall with constant heat flux [29] is:

$$\bar{\theta}_{H_{h,l}} \sim 2.34\phi^{0.3}\frac{L}{H}(Ra_{h,l}\,Pr)^{-1/5}Da^{-1/10} \quad (18)$$

where in here the high-heating and low-heating instantaneous Rayleigh numbers, Ra_h and Ra_l, are equal to $(1+A/2)Ra$ and $(1-A/2)Ra$, respectively (note: $Ra_{h,l} = Ra\,Q''$).

The two velocity equations, obtained from combining equations (17) and (18), and equation (14) form a system of algebraic and coupled non linear equations in the unknowns $F_v = 1/(2\Omega)$, V_h and V_l. The system of equations is solved numerically for each particular set of parameters.

Considering now a clear fluid configuration, the corresponding heating wall temperature scale and corresponding velocity scale equations are:

$$\bar{\theta}_{H_{h,l}} \sim \frac{L}{H}Ra_{h,l}^{-1/5}\xi(Pr)^{1/5} \quad (19)$$

$$V_{h,l}^2[1+Pr\,\xi(Pr)]+V_{h,l}\left[\frac{1}{\Omega}+\frac{1}{\Omega}Pr\,\xi(Pr)\right] - Ra\,Pr\,\xi(Pr)^{-1/2}\theta_{h,l} \sim 0. \quad (20)$$

Within the parametric range considered here, the numerical solution of the system of equations for clear fluid [equations (14), (19) and (20)], or porous medium [equations (14), (17) and (18)], configuration leads to four real theoretical solutions. Two of them were negative being immediately discarded. The correct answer, the resonance frequency, was selected among the remaining two by enforcing the positive velocity scale requirement (recall that the scale analysis is implicitly done along the heating wall where the fluid vertical velocity scale should be always positive). Only one of the two remaining solutions satisfied this requirement.

RESULTS AND DISCUSSION

The numerical scheme, presented in detail by Antohe and Lage [21], is based on the finite volume technique for solving the system of time dependent differential equations (1)–(4), with appropriate boundary and initial conditions. The present numerical code is validated against results reported by Armfield and Patterson [30]. Grid accuracy tests are performed, following the same basic concepts described in detail by Manole and Lage [31]. Several different grid distributions are implemented, depending on the case. Numerical results reported here are at least 5% accurate for a 50% increase in the total number of grid lines.

Numerical convergence is examined locally following the criterion

$$\max\left|\frac{\varepsilon^{i+1}-\varepsilon^{i}}{\varepsilon^{i}}\right| < 10^{-3} \quad (21)$$

where ε is replaced by U, V and θ at every (X, Y) location of the discretized domain, and i and $i+1$ are two consecutive iterations at the same time τ.

Numerical and theoretical resonance frequency results, with $L/H = 1$, $Pr = 7$, and heating amplitude A from 0.2 to 2.0, are presented in Table 1. Clear fluid results cover the Rayleigh number range 10^7–10^9. Porous medium results are obtained with $\phi = 0.4$, $\lambda = 0.4$, $J = 1$ and Darcy number 10^{-2}–10^{-6}. The Rayleigh number range for the porous medium cases is 10^6–10^8 for Darcy 10^{-2}, 10^{10}–10^{12} for Darcy 10^{-4}, and 10^{12}–10^{14} for Darcy 10^{-6}. Note that the corresponding porous-modified Rayleigh number (Ra_D) range is 10^4–10^6 for Darcy 10^{-2}, and 10^6–10^8 for Darcy 10^{-4} and 10^{-6}.

These parametric values are carefully selected. In all cases, for instance, the Rayleigh number varies from a low limiting value, below which flow resonance becomes undetectable, to a value limited by the required computational time for obtaining meaningful (accurate) results. The parameter λ/ϕ of equation (4) is equal to one, a reasonable approximation for values obtained in practical systems, e.g. glass–water = 1.33, soil–water = 1.24. From $(\rho c)_s = \phi(\rho c)_f + (1-\phi)(\rho c)_{matrix}$, it is straightforward to show that $\lambda = \phi$ is a limiting value valid for an adiabatic solid matrix. Therefore, the results presented here are valid also for concentration driven convection, if one replaces temperature with concentration, and thermal parameters with the corresponding solutal parameters.

As expected, the theoretical values are within a factor of order 1 from the numerical results, being consistently smaller. These results are remarkable considering that the theoretical approach is based on the linearization of all derivative terms in the transport equations, and that the flow inside the enclosure is highly complex and non linear.

The numerical simulations (presented later on) revealed that the resonance frequency is independent of the heating amplitude. The theoretical results are consistent with this assertion as indicated by the limited effect (maximum of 10%) of the heating amplitude on the resonance frequency, except for the particular case of $A = 2$. As mentioned previously, the low-heating period with $A = 2$ is in fact an adiabatic period (zero heat flux). The theoretical analysis predicts a zero scale for the flow velocity during this period, and this value is used when computing the resonance frequency. This is not realistic as the flow inertia induced during the high-heating period guarantees a different than zero flow speed during the adiabatic period. Therefore, a larger discrepancy between theoretically predicted and numerically obtained resonance frequencies for $A = 2$ is justified. The flow inertia effect is expected to be reduced when dealing with a porous medium system. This is con-

Table 1. Numerical results and theoretical predictions of the resonance frequency, F_v, for clear fluid and fluid saturated porous medium systems as a function of heating amplitude A

A	F_v	Clear fluid			$Da = 10^{-2}$			$Da = 10^{-4}$		
		$Ra = 10^7$	$Ra = 10^8$	$Ra = 10^9$	$Ra = 10^6$	$Ra = 10^7$	$Ra = 10^8$	$Ra = 10^{10}$	$Ra = 10^{11}$	$Ra = 10^{12}$
	num.	250	588	1666	33	114	294	1220	4000	10000
0.2	theo.	120.5	302.8	760.6	18.8	48.3	121.7	567.8	1497.5	3832.0
0.4	theo.	120.7	303.3	761.9	18.7	48.0	120.8	562.6	1484.5	3799.2
0.8	theo.	121.6	305.5	767.5	18.5	47.5	119.4	553.8	1462.1	3742.3
1.2	theo.	123.5	310.2	779.2	18.5	47.2	118.4	546.6	1443.8	3695.0
1.6	theo.	127.6	320.5	805.0	18.7	47.4	118.2	541.4	1429.9	3657.7
1.8	theo.	132.4	332.5	835.3	19.1	48.1	119.1	540.5	1426.8	3646.4
2.0	theo.	61.6	154.6	388.5	16.8	44.0	112.4	529.5	1402.2	3597.0

$L/H = 1$, $Pr = 7$ (for porous configuration: $\phi = 0.4$, $J = 1$, $\lambda = 0.4$).

firmed by the progressive smaller discrepancy between results of $A = 2$ and results of $A \neq 2$, for $Da = 10^{-2}$ and $Da = 10^{-4}$.

Particularly for the porous medium configuration, results of the low permeability case (Darcy equal to 10^{-6}) are not reported simply because no resonance is detected, even for Rayleigh number as high as 10^{14}. The sharp increase in resonance frequency as Darcy number varies from 10^{-2} to 10^{-4}, as shown in Table 1, indicates that a further reduction in Darcy number would require an even larger heating frequency for achieving resonance. This frequency seems be too large for the flow to respond under such high damping conditions (drag imposed by porous matrix).

Figures 2 and 3 present the time evolution of the thermal parameters, Nusselt numbers and hot wall averaged temperature [equations (9)–(11)], for $Ra = 10^8$ and $Da = 10^{-2}$, and for $Ra = 10^{12}$ and $Da = 10^{-4}$, respectively, and $A = 0.4$, 0.8 and 1.6 (from top to bottom). The graphs in each figure are for resonance frequency: $F = 294$ (Fig. 2) and $F = 10^4$ (Fig. 3).

In all cases, the mid plane Nusselt number, Nu_M, evolves to a periodic regime with amplitude larger than the heating amplitude. The amplitude difference increases with the heating amplitude. It seems that the heating amplitude, at resonance frequency, affects only the magnitude of the Nusselt number and the hot wall temperature value: neither the phase shift nor the frequency of response are changed. This is confirmed by the results presented in Fig. 4 (for $Da = 10^{-2}$) where the maximum mid-plane Nusselt number amplitude, $Nu_{M,max}$, is presented as function of frequency, F, for different heating amplitudes. Several local $Nu_{M,max}$ maxima are revealed. It was observed that the number and magnitude of these local maxima increase with the Rayleigh number and with the heating amplitude. The frequency for maximum $Nu_{M,max}$ is defined as the resonance frequency of the system. The other local maxima are developed at frequencies factor of the resonance frequency (harmonics), as expected. The resonance frequency and its harmonics, for any specific Rayleigh number, do not change with the heating amplitude. Beyond the resonance frequency the Nusselt number amplitude decays

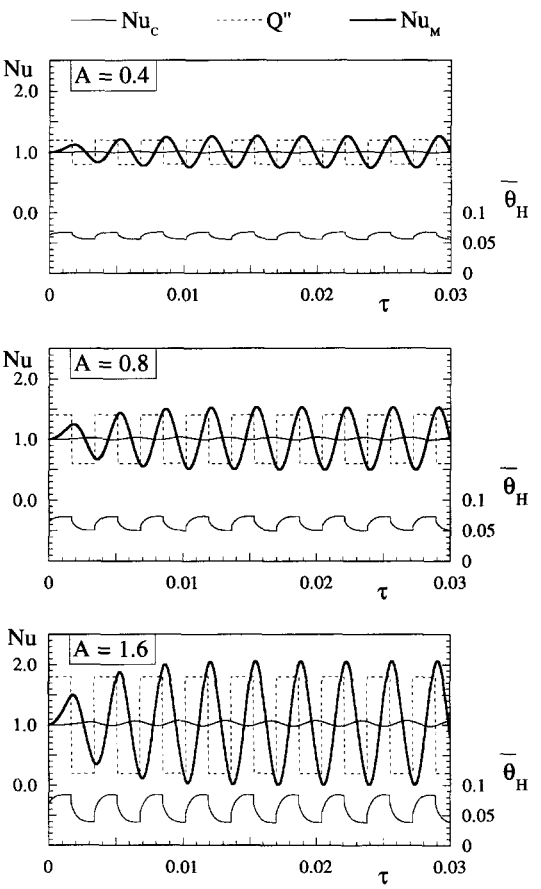

Fig. 2. Nusselt numbers and hot-wall-averaged temperature vs time: porous medium system, heating at resonance frequency $F = 294$, $Ra = 10^8$ and $Da = 10^{-2}$.

abruptly, indicating that the fluid is no longer capable of responding to the high frequency heating. In the limit of low frequencies, $Nu_{M,max}$ tends to A, the heating amplitude.

Some results of numerical simulations considering a clear fluid system are shown in Fig. 5. The graphs, for $Ra = 10^9$, resonance frequency $F = 1666$ and $A = 0.2$, 0.8 and 2.0 (from top to bottom), show a similar evolution in time as compared with results for the porous medium system. The evolution to steady

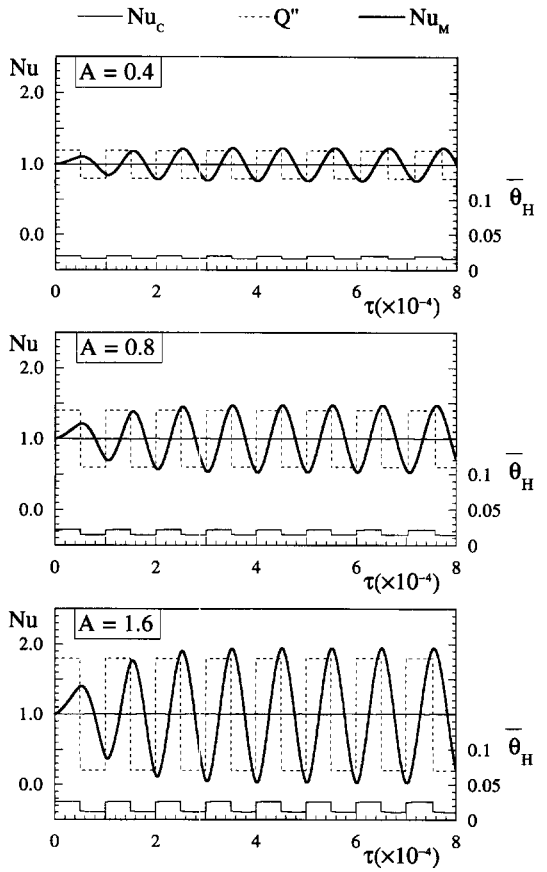

Fig. 3. Nusselt numbers and hot-wall-averaged temperature vs time: porous medium system, heating at resonance frequency $F = 10^4$, $Ra = 10^{12}$ and $Da = 10^{-4}$.

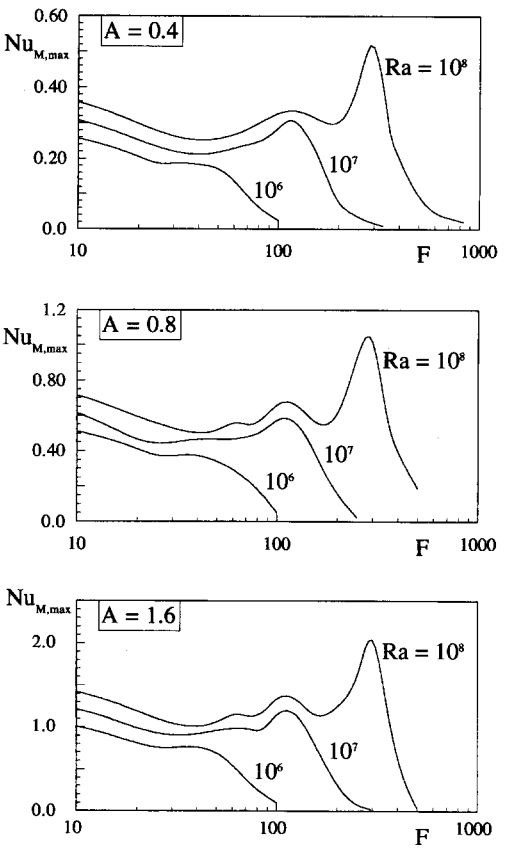

Fig. 4. Resonance amplitude, $Nu_{M,max}$, vs frequency for porous medium system with $Da = 10^{-2}$.

periodic regime requires a larger number of cycles in the clear fluid case than in the porous medium case. This phenomena is inertia related, and can be explained by the damping effect that a porous matrix imposes on the circulating flow due to viscous and form drags. The same effect accounts for the larger number of local maxima in the $Nu_{M,max}$ curves for the clear fluid configuration, presented in Fig. 6. The frequencies related with these maxima, harmonics of the resonance frequency, are Rayleigh-number dependent, which differs from the porous medium case.

Figure 7 presents a synthesis of the clear fluid and porous medium numerical simulations at the resonance frequency, with $Nu_{M,max}$ plotted as a function of the heating amplitude for clear fluid (top), porous medium with $Da = 10^{-2}$ (middle), and porous medium with $Da = 10^{-4}$ (bottom). The response of the system to changes in the heating amplitude is essentially linear: for the porous medium case and $Ra = 10^8$, the $Nu_{M,max}$ varies from 0.52 for $A = 0.4$ to 2.1 for $A = 1.6$, that is roughly a four fold increase in both $Nu_{M,max}$ and A; in the clear fluid case and $Ra = 10^9$, $Nu_{M,max}$ varies from 0.40 for $A = 0.2$, to 4.6 for $A = 2.0$, a 10 fold increase in both quantities. A general correlation is obtained for predicting the resonance amplitude, $Nu_{M,max}$, as function of heating amplitude, Rayleigh number and Darcy number:

$$Nu_{M,max} = \left[0.055 - \frac{0.0037}{(Ra^{0.05}Da)^{0.317}}\right] A\, Ra^{0.18}. \quad (22)$$

For the clear fluid system, the second term within brackets goes to zero.

Graphs of transients and phase-plane portraits are constructed for studying the heating amplitude effect on the evolution of the transport phenomena within the enclosure. Figure 8 presents the results for clear fluid system configuration, at resonance frequency, $Ra = 10^9$, and heating amplitude equal to $A = 0.2$ (top) and $A = 2.0$ (bottom). Each plot combines the time series of the hot-wall-averaged temperature with a phase-plane portrait of the hot-wall-averaged temperature vs a non-dimensional volume-averaged velocity, defined as

$$W = \frac{1}{(HL)} \sum_{i,j} \vartheta_{ij} (U(i,j)^2 + V(i,j)^2)^{1/2}. \quad (23)$$

The parameter ϑ_{ij} in equation (23) is the volume of the (i,j) local control volume. The volume averaged velocity provides a measure of the flow intensity inside the system.

Both phase-plane portraits show a steady-periodic

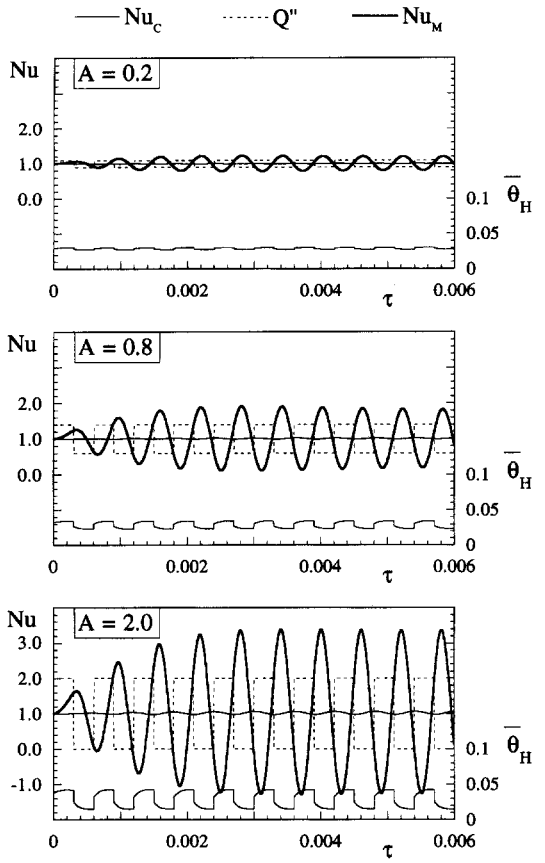

Fig. 5. Nusselt numbers and hot wall averaged temperature vs time: clear fluid system, heating at resonance frequency $F = 1666$ and $Ra = 10^9$.

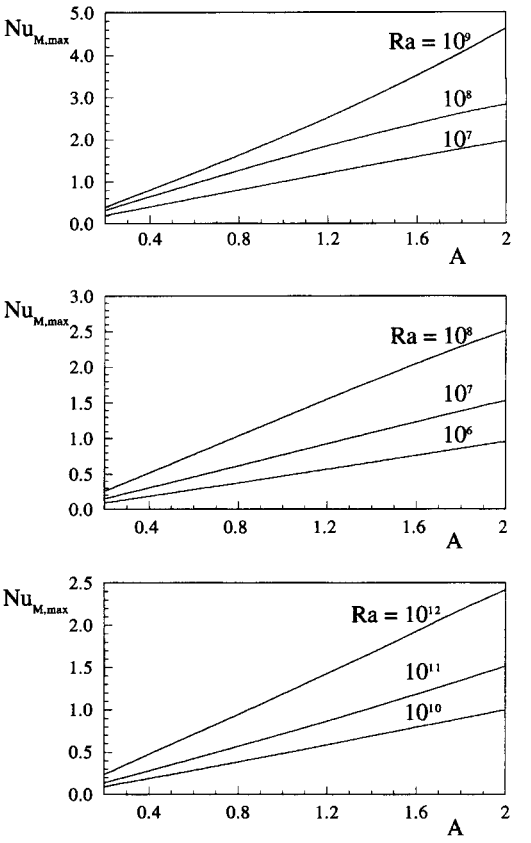

Fig. 7. Resonance amplitude, $Nu_{M,max}$, vs heating amplitude for clear fluid system (top), and for porous systems with $Da = 10^{-2}$ (middle) and $Da = 10^{-4}$ (bottom): summary of numerical results.

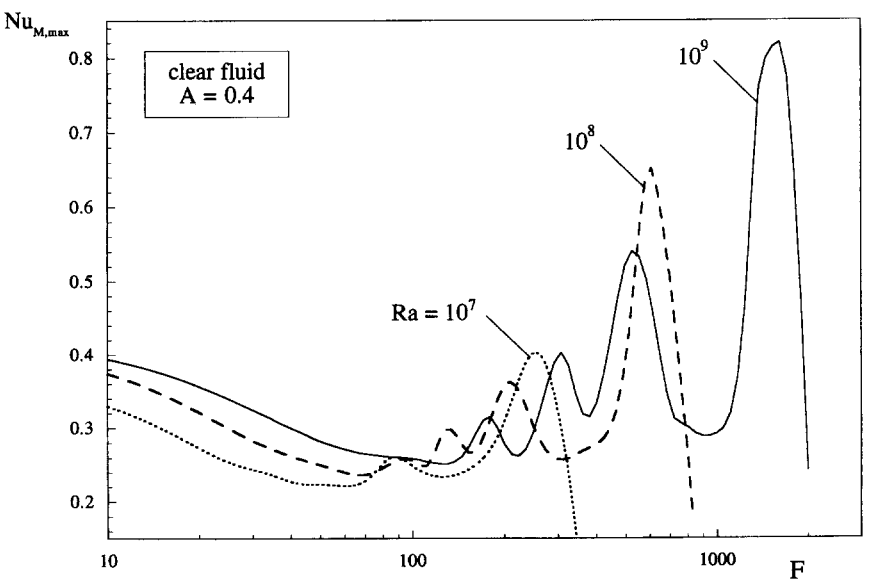

Fig. 6. Resonance amplitude, $Nu_{M,max}$, vs frequency for clear fluid system.

regime. The black dots are numbered following the heating process, with 1 representing the beginning of the high-heating cycle. The hot-wall-averaged temperature evolution follows to a good extent the heating cycle, approaching an asymptotic value at the end of the high-heating and low-heating periods: points 3 and 6 for $A = 0.2$, and points 7 and 12 for $A = 2$. Some peculiarities, however, can be observed immedi-

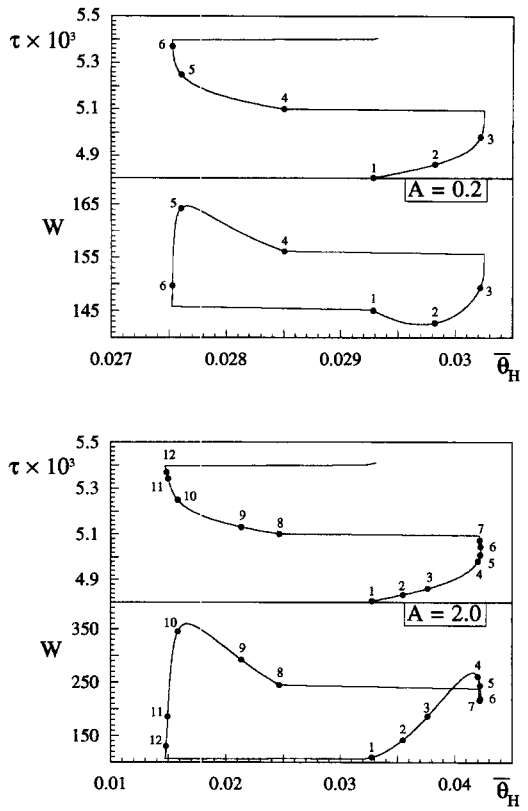

Fig. 8. Time-periodic (cyclic) evolution of wall averaged temperature and phase-plane portraits for a clear fluid system heated at resonance frequency, and $Ra = 10^9$: heating amplitude effect.

ately in the phase-plane portrait graphs. In the top plot ($A = 0.2$), for instance, the average velocity decreases during the initial high-heating period (from 1 to 2) and then it increases during the low-heating cycle, from 4 to 5, two somewhat unexpected results. In the lower plot ($A = 2$), the velocity reduction happens at the end of the high-heating period, from 4 to 7, and again a velocity increase is noticed during the low-heating regime. Cases with heating amplitude in between 0.2 and 2 show transition of velocity behavior from the behavior at amplitude 0.2 to the one at 2.

The corresponding streamline frames, with stream function defined as $U = \partial\Psi/\partial Y$ and $V = -\partial\Psi/\partial X$, are presented in Fig. 9, for $A = 0.2$, and Fig. 10, for $A = 2.0$. Minimum and maximum streamfunction values are fixed when plotting the frames of each figure. The arrows indicate the rotation of the fluid.

Following side-to-side the streamline evolution and the averaged velocity evolution, the case of $A = 0.2$ is first analyzed. The reduction in the average velocity from 1 to 2 is caused by the formation of counter-rotating cells inside the enclosure. The step increase in the heat flux applied to the right wall (hot wall) accelerates a fluid pack next to it. This fluid pack rises, reaches the top of the enclosure and then it turns left facing a slow moving fluid pack, one that was moving along the right wall during the previous low-heating period. The fast fluid pack then chooses a less resistive path, flowing downwards to the center of the enclosure instead of going all the way to the left wall. A counter-clockwise cell is formed in 2, opposite to the flow cell adjacent to the left wall (cold wall). It is the shear competition (momentum diffusion) of these counter rotating cells that is responsible for the decrease in the averaged velocity during the initial high-heating regime. A similar argument explains the velocity increase from 4 to 5. In this case, as seen by the streamlines, the flow inertia built up during the high-heating period forces the merging of the two counter-rotating cells (notice from frame 3 to 4 how the right wall cell protruded towards the left wall). A unique large cell, in frame 5, occupies the entire enclosure with the flow assuming a well organized form. Evidently, the following low-heating regime provides a thermo-brake for the fluid, reducing the average velocity from 5 to 6.

The $A = 2.0$ case reveals a different, and more complex, flow structure. From frame 1 to frame 4 of Fig. 10, several cells are present, all co-rotating cells, and the averaged velocity keeps increasing (Fig. 8, bottom). The buoyancy induced during the high-heating regime, starting at 1, accelerates the fluid flowing along these cells. These cells behave as momentum transmission gears. From 4 to 7, the right upper corner jet formed by the accelerated fluid, protrudes itself towards the left side wall, tending to take over the entire enclosure. At frame 5, lower and upper branches managed to cross the entire enclosure creating zones of counter-current flow. That is why the average velocity value declines (Fig. 8). From frames 8 to 10, again a unique flow cell fills the enclosure propitiating a more organized flow wheel and an increase in the averaged velocity. At frames 11 and 12, the separation of the boundary layer along the right wall with the formation of a clockwise cell is evident. This is the breaking effect provided by the switch from high-heating to low-heating period.

Another very interesting point, in agreement with previous observation [21], is the strong thermal stratification present at the center of the enclosure throughout the heating process. The isotherms (not included) show very little variation, even with such complex flow structures as presented in Fig. 10.

A final note is the observation that a large portion of the fluid inside the enclosure travels a distance smaller than the perimeter of the enclosure during a heating cycle. This indicates, with equation (13), that the theoretically predicted resonance frequency is a lower bound for the actual resonance frequency, in support of the results presented in Table 1.

DIMENSIONAL RESULTS

Some dimensional configurations are now exemplified, and the numerical results translated into dimensional quantities. Keep in mind that the number

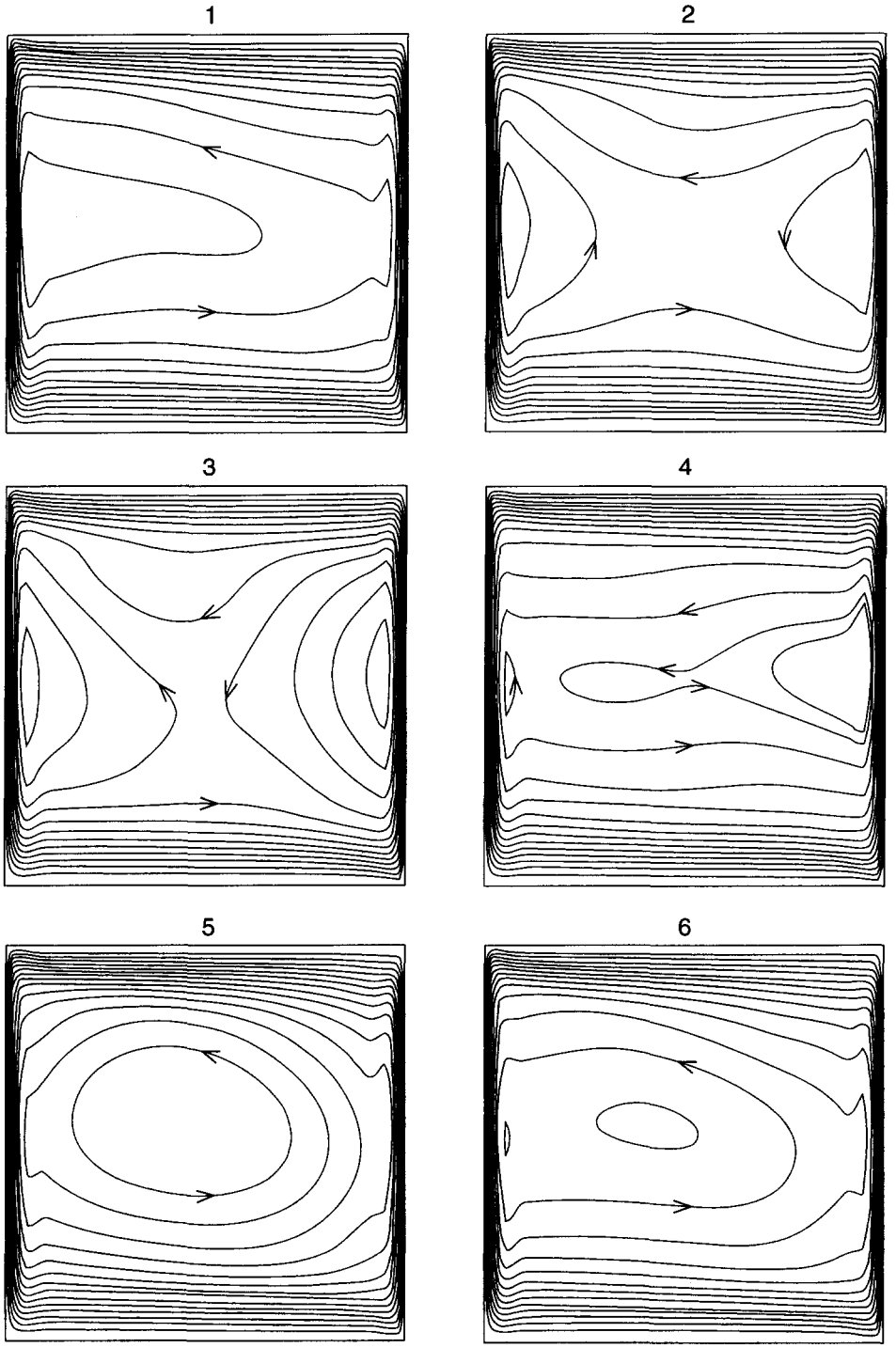

Fig. 9. Streamlines corresponding to top plot of Fig. 8 : $A = 0.2$.

of possible practical configurations leading to non-dimensional parameters within the range presented here is unlimited ; this is the beauty of dimensional results!

For the clear fluid configuration, one can consider an enclosure with characteristic dimension around 0.1 m, for instance. A heat flux of the order of 50 W m^{-2} leads to $Ra \sim 10^9$. The critical dimensionless frequency for this particular case is about 600 (Table 1), or a dimensional pulsating period of about 50 s. For the porous medium case, consider a 0.1 m high polyethylene foam enclosure (permeability around 10^{-6} m^2) saturated with water. Rayleigh number around 10^{10} is obtained with a heat flux of 2 kW m^{-2}. The numerical results (Table 1) predict resonance frequency around 1200 or dimensional pulsating period of 30 s.

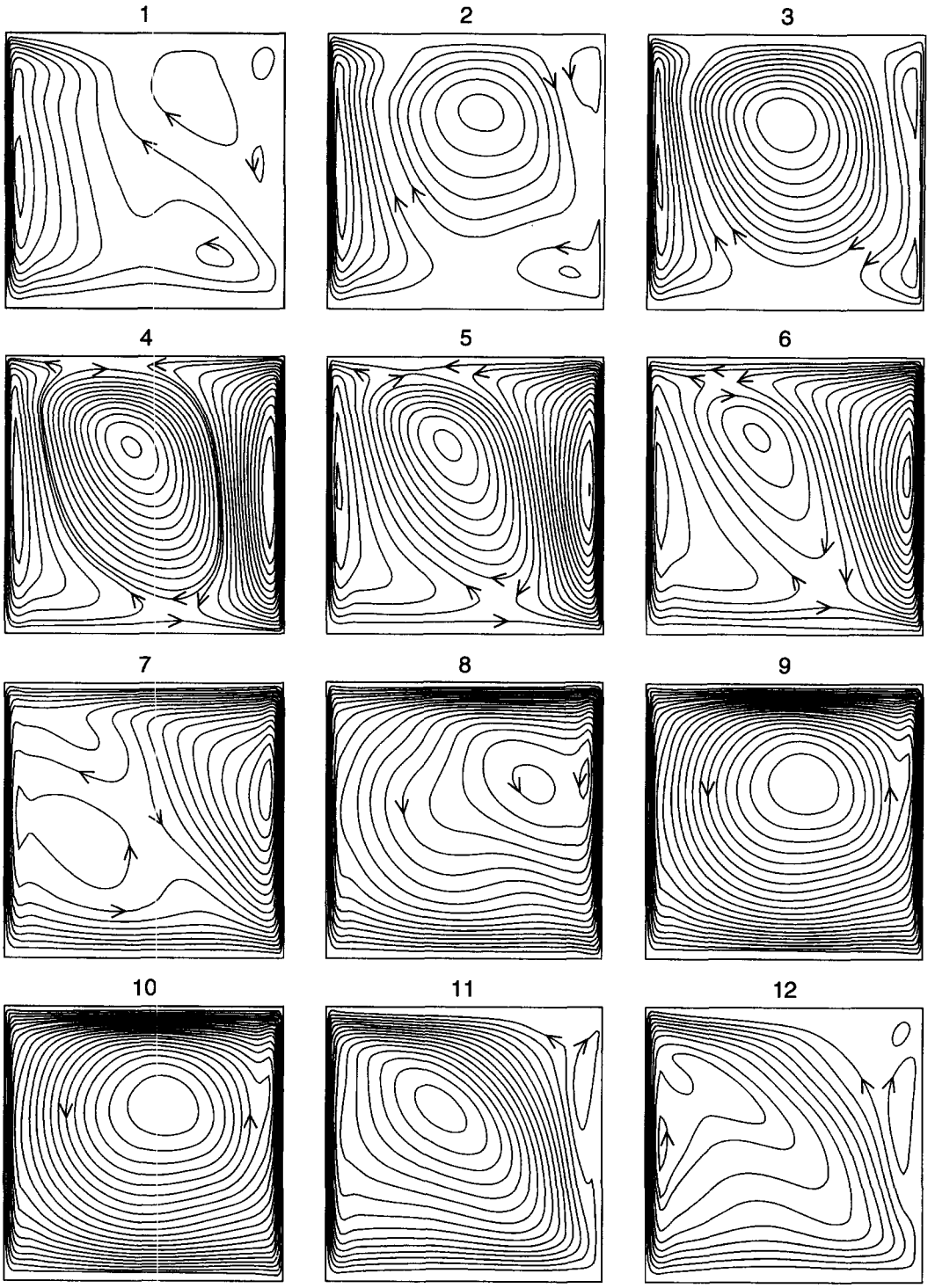

Fig. 10. Streamlines corresponding to bottom plot of Fig. 8: $A = 2.0$.

CLOSURE

Transport of momentum and heat are investigated theoretically and numerically considering clear fluid and fully saturated porous medium enclosures under time periodic heating in the horizontal direction.

The effects of heating amplitude and frequency on the transport phenomena are investigated in detail. A general theoretical model for predicting the natural frequency of the flow circulating inside a clear fluid, or porous medium, enclosure is obtained as a system of non-linear algebraic equations. This model, that incorporates the heating amplitude effect, is very important since flow resonance is believed to emerge

as the heating frequency matches the natural frequency of the flow wheel inside the enclosure.

Numerical simulations indicate that the natural convection activity within the enclosure reaches several local maxima (harmonics) as the heating frequency is increased, with a climax at a certain frequency referred to as *resonance frequency*. The theoretical estimates, consistently smaller than the numerical results, provide a powerful tool for guiding the numerical simulations towards a more precise determination of the resonance frequency.

The clear fluid system seems to be more sensitive to variations in the heating amplitude. The additional drag imposed by the solid matrix of a porous medium system damps the flow inertia reducing the flow resonance. No resonance is detected for systems with Darcy number smaller or equal to 10^{-6}.

The resonance frequency is shown to be independent of the heating amplitude for both clear fluid and porous medium configurations. Moreover, the natural convection response is shown to vary linearly with heating amplitude for a wide range of parameters, in agreement with theoretical predictions. A general correlation for determining the resonance amplitude, as function of Rayleigh number and Darcy number, is provided.

The effect of increasing the heating amplitude on the flow evolution during a heating cycle is analyzed in detail. Using time evolution graphs, phase-plane portraits, and streamlines, several peculiar aspects are highlighted and explained. The flow is in general highly complex with strong mixing and little effect on the isotherm distribution. The streamlines support the verification that the theoretical model offers a lower bound for the resonance frequency.

Acknowledgements—Financial support provided by NSF through grant no. CTS-9504968 is greatly appreciated. Mr Antohe expresses his gratitude for the Ph.D. scholarship provided by the Mechanical Engineering Department of Southern Methodist University. Professor Lage is grateful to the financial support provided by the J. L. Embrey Professorship in Mechanical Engineering.

REFERENCES

1. K. Vafai and H. C. Tien, A numerical investigation of phase change effects in porous material, *Int. J. Heat Mass Transfer* **32,** 1261–1277 (1989).
2. H. Yoo and R. Viskanta, Effect of anisotropic permeability on the transport process during solidification of a binary mixture, *Int. J. Heat Mass Transfer* **35,** 2335–2346 (1992).
3. I. F. Obinelo, G. F. Round, and J. S. Chang, Condensation enhancement by steam pulsation in a reflux condenser, *Int. J. Heat Fluid Flow* **15,** 20–29 (1994).
4. J. R. L. Skarda, Thermal modeling with solid–liquid phase change of thermal energy storage experiment, NASA-Lewis Research Center, Technical Memorandum 103770 (1991).
5. M. Chang, L. C. Chow, W. S. Chang and M. Morgan, Transient behavior of heat pipes with thermal energy storage under reversed-pulsed heat loads, *AIAA J. Thermophys. Heat Transfer* **6,** 685–692 (1992).
6. T. Yano, M. Ochi and S. Enya, Protection against fire and high temperature by using porous media and water, *ASME/JSME Thermal Engng Proc.* **4,** 213–218 (1991).
7. N. E. Wijeysundera and M. N. A. Hawlader, Effects of condensation and liquid transport on thermal performance of fibrous insulations, *Int. J. Heat Mass Transfer* **35,** 2605–2616 (1992).
8. J-P. Fohr and H. B. Mousa, Heat and mass transfer in a cylindrical grain silo submitted to a periodical wall heat flux, *Int. J. Heat Mass Transfer* **37,** 1699–1712 (1994).
9. Z. Zhang and A. Bejan, The horizontal spreading of thermal and chemical deposits in a porous medium, *Int. J. Heat Mass Transfer* **30,** 2289–2303 (1987).
10. T. Fusegi and J. M. Hyun, Laminar and transitional natural convection in an enclosure with complex and realistic conditions, *Int. J. Heat Fluid Flow* **15,** 258–268 (1994).
11. H. Q. Yang, K. T. Yang and Q. Xia, Periodic laminar convection in a tall vertical cavity, *Int. J. Heat Mass Transfer* **32,** 2199–2207 (1989).
12. M. Kazmierczak and Z. Chinoda, Buoyancy-driven flow in an enclosure with time periodic boundary conditions, *Int. J. Heat Mass Transfer* **35,** 1507–1518 (1992).
13. J. L. Lage and A. Bejan, The resonance of natural convection in an enclosure heated periodically from the side, *Int. J. Heat Mass Transfer* **36,** 2027–2038 (1993).
14. J. Mantle, M. Kazmierczak and B. Hiawy, The effect of temperature modulation on natural convection in a horizontal layer heated from below: high-Rayleigh-number experiments, *J. Heat Transfer* **116,** 614–620 (1994).
15. J. L. Lage, Convective currents induced by periodic time-dependent vertical density gradient, *Int. J. Heat Fluid Flow* **15,** 233–240 (1994).
16. J. P. Caltagirone, Stabilité d'une couche poreuse horizontale soumise a des conditions aux limites périodiques, *Int. J. Heat Mass Transfer* **19,** 815–820 (1976).
17. B. Chhuon and J. P. Caltagirone, Stability of a horizontal porous layer with timewise periodic boundary conditions, *J. Heat Transfer* **98,** 49–54 (1976).
18. N. Rudraiah and M. S. Malashetty, Effect of modulation on the onset of convection in sparsely packed porous layer, *J. Heat Transfer* **112,** 685–689 (1990).
19. M. Kazmierczak and A. Muley, Steady and transient natural convection experiments in a horizontal fluid layer: the effects of a thin top fluid layer and oscillating bottom wall temperature, *Int. J. Heat Fluid Flow* **15,** 30–41 (1994).
20. D. A. Nield, Onset of convection in a porous medium with nonuniform time-dependent volumetric radiation, *Int. J. Heat Fluid Flow* **16,** 217–222 (1995).
21. B. V. Antohe and J. L. Lage, A dynamic thermal insulator: inducing resonance within a fluid saturated porous medium enclosure heated periodically from the side, *Int. J. Heat Mass Transfer* **37,** 751–782 (1994).
22. K. Vafai and C. L. Tien, Boundary and inertia effects on flow and heat transfer in porous media, *Int. J. Heat Mass Transfer* **24,** 195–203 (1981).
23. C. T. Hsu and P. Cheng, Thermal dispersion in a porous medium, *Int. J. Heat Mass Transfer* **33,** 1587–1597 (1990).
24. P. Cheng, Heat transfer in geothermal systems, *Adv. Heat Transfer* **14,** 1–105 (1978).
25. S. Ergun, Fluid flow through packed columns, *Chem. Engng Prog.* **48,** 89–94 (1952).
26. J. L. Lage, Natural convection within a porous medium cavity: predicting tools for flow regime and heat transfer, *Int. Commun. Heat Mass Transfer* **20,** 501–513 (1993).
27. A. Bejan, *Convection Heat Transfer*. Wiley, New York (1984).
28. J. L. Lage, On the theoretical prediction of transient heat transfer within a rectangular fluid-saturated porous medium enclosure, *J. Heat Transfer* **115,** 1069–1071 (1993).

29. D. A. Nield and A. Bejan, *Convection in Porous Media*. Springer, New York, NY (1991).
30. S. W. Armfield and J. C. Patterson, Direct simulation of wave interactions in unsteady natural convection in a cavity, *Int. J. Heat Mass Transfer* **34,** 929–940 (1991).
31. D. M. Manole and J. L. Lage, Nonuniform grid accuracy test applied to the natural convection flow within a porous medium cavity, *Numer. Heat Transfer B* **23,** 351–368 (1993).